pp 1788–1810. © Royal Aeronautical Society 2018
doi:10.1017/aer.2018.99

Trajectory optimisation of six degree of freedom aircraft using differential flatness

P. Elango
purnanandelango@gmail.com
R. Mohan
Department of Aerospace Engineering,
Indian Institute of Technology Madras, Chennai, India

ABSTRACT

The flatness of a six-degree-of-freedom (6DoF) aircraft model with conventional control surfaces – aileron, flap, rudder and elevator, along with thrust vectoring ability is established in this work. Trajectory optimisation of an aircraft can be cast as an inverse problem where the solution for control inputs that yield desired trajectories for certain states is sought. The solution to the inverse problems for certain systems is made tractable when they exhibit differential flatness. Flatness-based trajectory optimisation has a significant advantage over an equivalent collocation-based method in terms of computational efficiency and viability for real-time implementation. An application for the flatness of 6DoF aircraft is shown in the trajectory optimisation for dynamic soaring, and its connection with an equivalent 3DoF flatness-based implementation is also brought out. The results are compared with that from a collocation-based approach.

Keywords: Differential flatness; Trajectory optimisation; 6DoF aircraft; Dynamic soaring

Received 8 February 2018; revised 4 July 2018; accepted 5 July 2018.

https://doi.org/10.1017/aer.2018.99 Published online by Cambridge University Press

NOMENCLATURE

b	wing span (m)
c	reference chord length (m)
$\mathbf{c}(\mathbf{z})$	vector of inequality constraints
$C_{(\cdot)}$	cosine of an angle
$\bar{C}_{D0}$	average contribution of control surface deflections to C_D
C_{D0}, $C_{\Upsilon 0}$, C_{L0}	intercept terms in the expression of C_D, C_Υ and C_L, respectively
$C_{D(\cdot)}$, $C_{\Upsilon(\cdot)}$, $C_{L(\cdot)}$	derivatives of the aerodynamic force coefficients with respect to $(\cdot)$
$C_{l(\cdot)}$, $C_{m(\cdot)}$, $C_{n(\cdot)}$	derivatives of the aerodynamic moment coefficients with respect to $(\cdot)$
C_{Tx}, C_{Ty}	components of the vectored thrust (normalised with QS) along the body x and y axes, respectively
d	distance between the CG and the propeller along the body x-axis (m)
$\mathbf{d}$, $\mathbf{b}_0$, $\mathbf{b}_{si}$, $\mathbf{b}_{ci}$	coefficient vectors in the Fourier series expansion of the flat outputs ($i = 1,\ldots, M$), belonging to $\mathbb{R}^6$
D, L	aerodynamic drag and lift force in the wind axes (N)
$\mathbf{f}$	force on the aircraft in the body frame, acting at the CG (N)
g	acceleration due to gravity at sea-level, 9.806 m/s^2
$\mathbf{g}$	vector field representing the right-hand side of the state-space form of the 6DoF equations of motion
$\mathbf{h}$	smooth vector field
H_R	reference altitude, 20 m
i, j, k	natural numbers
$\mathbf{I}$	mass moment of inertia matrix (kg m^2)
$\mathbf{l}_b$, $\mathbf{u}_b$	vector of lower bound and upper bound on $\mathbf{z}$, respectively
$\mathcal{L}, \mathcal{M}, \mathcal{N}$	roll, pitch and yaw moment – aerodynamic moments in the wind axes (N m)
m	mass of the aircraft (kg)
M	number of harmonics in the Fourier series representation of the flat outputs
n	load factor
N	number of points within [0, t_f] where constraints are imposed during optimisation
$\mathbf{m}$	moment on the aircraft in the body frame, acting about the CG (N m)
$\mathfrak{p}$	exponent in the wind model, 0.25
$[p\ q\ r]^T$	components of the body frame angular velocity along the body axes (rad/s)
Q	dynamic head (N/m^2)
$\mathbb{R}$	set of real numbers
S	reference surface area (m^2)
$S_{(\cdot)}$	sine of an angle
$\mathbf{S}$	matrix for transforming from the inertial frame to the body frame
t_f	time of flight (s)
$[u\ v\ w]^T$	components of the relative wind velocity along the body axes (m/s)
$\mathbf{u}$	vector of control inputs
V_R	wind speed at reference altitude H_R (m/s)
V_T	aircraft's total airspeed (m/s)
$[W_x\ W_y\ W_z]^T$	components of wind velocity along the inertial axes (m/s)
W_{xz}	$\partial W_x/\partial z$ (per second)

https://doi.org/10.1017/aer.2018.99 Published online by Cambridge University Press

$[x\ y\ z]^T$	co-ordinates of the aircraft's CG in an inertial frame (m)
(X, Y, Z)	inertial frame axes
(X_b, Y_b, Z_b)	body frame axes
$\mathbf{x}$	vector of state variables
$\mathbf{y}$	vector of flat outputs
$\mathbf{y}^{(k)}$	k^{th} time derivative of $\mathbf{y}$
$\mathbf{z}$	vector of design variables

Greek Symbol

α, β	angle of attack and side-slip angle (rad)
$\delta_f, \delta_a, \delta_e, \delta_r$	flap, aileron, elevator and rudder deflection, respectively (rad)
$\boldsymbol{\zeta}, \boldsymbol{\xi}$	smooth vector fields
κ	natural number
ρ	air density at sea-level, 1.225 kg/m^3
$\boldsymbol{\varphi}$	wind velocity expressed along the body axes (m/s)
ϕ, θ, ψ	Euler angles of the body axes (rad)
$\boldsymbol{\Upsilon}$	aerodynamic side-force in the wind axes (N)

Superscript

$\dot{(\,)}, \ddot{(\,)}$	first- and second-time derivatives, respectively

Subscript

$(\cdot)_{\text{avg.}}$	average of $(\cdot)$ over $[0, t_f]$

Abbreviations

AVL	Athena Vortex Lattice
CG	centre of gravity
DoF	degree of freedom
UAV	unmanned aerial vehicle

1.0 INTRODUCTION

The problem of solving the inverse dynamics of a system constitutes the determination of control inputs such that one or more states of the system follow a desired trajectory. A number of studies in the recent past have investigated the scope of treating flight control and trajectory optimisation as an inverse problem. Thomson and Bradley[1] provide a comprehensive overview of the pioneering contributions that have been made in this field of research.

Obtaining the solution to an inverse problem is by no means trivial. Design of most controllers aims to exploit a certain nuanced property of the system to be controlled. A class of nonlinear systems exhibits a property called differential flatness which makes their inverse simulation immensely tractable. A system is flat if we can find a set of outputs (equal in number to the number of inputs) such that all states and inputs can be determined from these outputs and their time derivatives without integration[2]. Flatness-based control was originally

https://doi.org/10.1017/aer.2018.99 Published online by Cambridge University Press

introduced by Fliess et al.[3], and its application to trajectory optimisation was explored by Nieuwstadt and Murray[4]. Since the behaviour of the flat system is governed by the flat outputs, flatness is particularly advantageous for trajectory optimisation. Trajectories planned in the output space can be mapped to the state and the input space algebraically. Moreover, this mapping significantly lowers the dimensionality of the problem. In the context of trajectory optimisation, direct collocation treats all the states and inputs at discrete locations as design variables, whereas in flatness-based methods, it is sufficient to optimise only the flat outputs. Unlike the former, where the derivatives of the states are not required, the success of flatness-based methods is hinged on the accurate estimation of the derivatives of the flat outputs. Once this bottleneck is addressed, flatness-based methods can outperform their collocation-based counterparts in terms of efficiency and viability for real-time implementation[5].

When one is interested in obtaining near-optimal solutions, trajectory optimisation can be performed by parameterising the flat outputs with differentiable basis functions. Such a parameterisation allows the accurate computation of the derivatives and it becomes possible to obtain a closed form expression for the various control inputs of the system. Yakimenko[6] has described such a procedure for three-degree-of-freedom (3DoF) aircraft dynamics using a polynomial parameterisation.

In this work, the flatness of a 6DoF aircraft model is demonstrated and is used for obtaining periodic dynamic soaring trajectories. An aircraft engaged in dynamic soaring extracts energy from a wind gradient field for the purpose of enhancing its endurance. Numerous studies in the recent past have investigated trajectory optimisation for dynamic soaring, mostly on a 3DoF aircraft model. Of these, Deittert et al.[7], and Akhtar et al.[8], have employed a flatness-based approach. The former has used a Fourier series representation for the flat outputs while the latter has followed the approach outlined in Yakimenko[6].

Very few works have addressed the related 6DoF problem. While the 3DoF dynamic soaring solution has been used to simulate the 6DoF aircraft's trajectory and attitude in several works[9–11], not many have investigated the 6DoF trajectory optimisation. Flanzer et al.[12] have used a compact vortex lattice method (CVLM) for computing the aerodynamic forces and moments, and have obtained travelling dynamic soaring trajectories using direct collocation. Liu et al.[13] have demonstrated a piece-wise guidance and control strategy by means of a flight simulation platform for dynamic soaring. A flatness-based formulation using the 6DoF model, however, has not yet been explored.

Martin[14] is the first to offer a perspective into the flatness of 6DoF aircraft dynamics by proposing a controller design. The equations of motion are split into three parts based on the time-scales involved and each of the three is controlled separately. The aircraft's inertial frame co-ordinates and the side-slip angle serve as the flat outputs. Four control inputs are incorporated into the model – three conventional control surfaces (aileron, rudder and elevator) and longitudinal thrust. The aerodynamic forces and moments are estimated using a look-up table[15] that spans across operating points. The control surface deflections are assumed to affect only the aerodynamic moments and not the forces. A few subsequent studies[16,17] have adapted the approach due to Martin[14] for various applications.

The recipe for the flatness of 6DoF aircraft proposed in this work differs from the prior analyses in two respects. The aircraft's inertial frame position and its body axes Euler angles are treated as flat outputs. Flaps and thrust vectoring are incorporated in addition to the inputs considered in Martin's work. Second, the use of a look-up table in the midst of trajectory optimisation or tracking is computationally expensive. Hence, it is preferable to

https://doi.org/10.1017/aer.2018.99 Published online by Cambridge University Press

possess a low-order functional form for the aircraft's aerodynamics without compromising on the accuracy. In the present formulation, the aerodynamic forces and moments are estimated from the widely used coefficient build-up[18,19] method involving stability and control derivatives, which are computed at a nominal representative flight condition. In contrast to Martin's approach, this linearized aerodynamics model accounts for the effect of the control surfaces on both forces and moments. During the estimation of the control inputs, it is assumed that the aircraft is in co-ordinated flight and the angle of attack is constrained to remain in the regime where linearity is valid. These constraints are fairly easy to impose during optimisation.

The model of an aircraft could be enhanced by accounting for the dynamics of the control surface actuators. However, the time-scale associated with the actuator mechanism is typically much smaller than the other time-scales of aircraft dynamics. Therefore, it is reasonable to ignore the actuator mechanisms and assume that the commanded deflections are achieved instantaneously for simplicity.

A study by Sequeira et al.[20] showed that flight simulations employing stability derivatives-based aerodynamic model were in good agreement with higher fidelity flight simulations that accounted for the unsteady effects as long as the bounds within which the quasi-steady assumptions hold were not violated.

In the succeeding sections, flatness of a 6DoF aircraft model is illustrated and subsequently applied to dynamic soaring trajectory optimisation. The optimisation problem is implemented in the presence of appropriate constraints that ensure the validity of the flatness analysis. A connection is highlighted between the 6DoF flatness-based implementation and its equivalent 3DoF counterpart. Also, the results from the flatness and collocation-based optimisation are compared.

2.0 AIRCRAFT MODEL

The aircraft model considered in this analysis is a small-scale UAV which is created based on the guidelines followed in Deittert et al.[7] and Bower[21]. It possesses the attributes of a high aspect-ratio sailplane designed for soaring and has the capacity to vector its thrust in the x–y plane (Fig. 1). This model accounts for six control inputs as mentioned previously. The essential parameters of the aircraft are summarised in Table 1. The stability and control derivatives of the aircraft given in Table A1 are used in the computation of aerodynamic coefficients (8). These are estimated using AVL[22] for a level trimmed flight at a nominal airspeed of 20 m/s. The nominal airspeed is obtained from the solution to the 3DoF trajectory optimisation. It represents the aircraft's mean airspeed across the duration of the manoeuvre.

3.0 EQUATIONS OF MOTION

Three co-ordinate frames are required for developing the aircraft's equations of motion – the Earth-fixed inertial frame, the wind frame and the body-fixed frame. The standard north-east-down co-ordinate axes are used for each of the frames. The body axes, inertial axes and the orientation of the relative wind perceived by the aircraft are depicted in Fig. 2.

Dynamic soaring manoeuvres require the presence of wind shear. So a steady wind whose strength varies exponentially with altitude is assumed to blow along the positive x-axis of the inertial frame as shown in (1). The exponential model provides a fairly good representation of

https://doi.org/10.1017/aer.2018.99 Published online by Cambridge University Press

Table 1
Aircraft parameters

Property	Value
Mass, m (kg)	4.5
Ref. span, b (m)	3
Ref. chord, c (m)	0.161
Ref. area, S (m^2)	0.473
d (m)	0.115
Moment of Inertia, I_x (kg m^2)	1.4
I_y (kg m^2)	0.9
I_z (kg m^2)	2.3
I_{xz} (kg m^2)	0.05
All other products of inertia	0

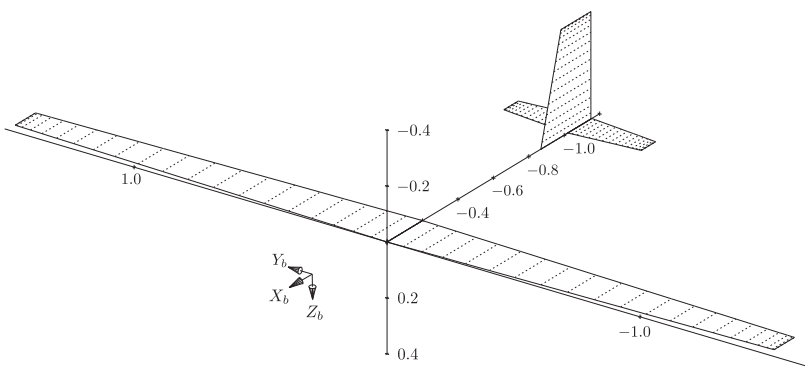


Figure 1. Aircraft geometry generated in AVL.

the wind speed in the atmospheric boundary layer near the ground and it has been employed in several prior studies of dynamic soaring[7,23,24]. In (1), V_R is the wind speed at a reference altitude H_R and it denotes the strength of the wind field. During trajectory optimisation, V_R is a design variable while H_R and $\mathfrak{p}$ are constants, 20 m and 0.25, respectively, adopted from Liu et al.[23]:

$$W_x = V_R\left(\frac{-z}{H_R}\right)^{\mathfrak{p}} \qquad ...(1)$$

The relationship between the components of the relative wind velocity along the body axes and the aircraft's velocity in the inertial frame is given by (2). The components of the wind velocity along the body axes are represented by $\boldsymbol{\varphi}$ (A.3) and the matrix $\mathbf{S}$ (A.2) transforms the inertial axes quantities to the body axes:

$$\begin{bmatrix}\dot{x}\\ \dot{y}\\ \dot{z}\end{bmatrix} = \mathbf{S}^T\left(\begin{bmatrix}u\\ v\\ w\end{bmatrix} + \boldsymbol{\varphi}\right) \qquad ...(2)$$

https://doi.org/10.1017/aer.2018.99 Published online by Cambridge University Press

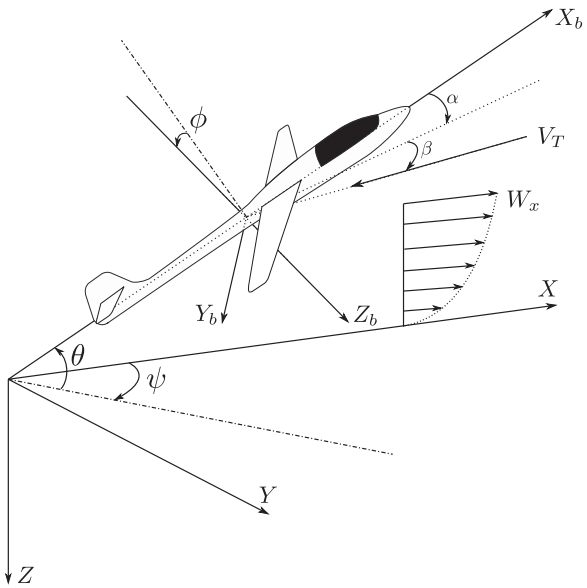


Figure 2. Depiction of the various co-ordinate frames.

Rearrangement of the time derivative of (2) yields us (3) and (4), which concern the forces on the body and the rate of change of the components of the relative wind along the body axes:

$$\begin{bmatrix} \dot{u} \\ \dot{v} \\ \dot{w} \end{bmatrix} + \mathbf{S}\dot{\mathbf{S}}^T \begin{bmatrix} u \\ v \\ w \end{bmatrix} = \frac{\mathbf{f}}{m} + \mathbf{S} \begin{bmatrix} 0 \\ 0 \\ g \end{bmatrix} - \mathbf{S} \begin{bmatrix} W_{xz}\dot{z} \\ 0 \\ 0 \end{bmatrix} \quad \ldots(3)$$

$$\mathbf{f} = \begin{bmatrix} F_x \\ F_y \\ F_z \end{bmatrix} = m \left(\begin{bmatrix} \dot{u} \\ \dot{v} \\ \dot{w} \end{bmatrix} + \begin{bmatrix} wq - vr \\ ru - pw \\ pv - qu \end{bmatrix} - g \begin{bmatrix} -S_\theta \\ C_\theta S_\phi \\ C_\theta C_\phi \end{bmatrix} + W_{xz}\dot{z} \begin{bmatrix} C_\psi C_\theta \\ C_\psi S_\theta S_\phi - S_\psi C_\phi \\ C_\psi S_\theta C_\phi + S_\psi S_\phi \end{bmatrix} \right) \quad \ldots(4)$$

The relationship between the body frame angular velocity and the rate of change of the Euler angles is given by (5). This, along with the Euler equations of motion defines the rotational dynamics of the aircraft in (6, 7):

$$\begin{bmatrix} \dot{\phi} \\ \dot{\theta} \\ \dot{\psi} \end{bmatrix} = \begin{bmatrix} 1 & S_\phi \tan\theta & C_\phi \tan\theta \\ 0 & C_\phi & -S_\phi \\ 0 & S_\phi \sec\theta & C_\phi \sec\theta \end{bmatrix} \begin{bmatrix} p \\ q \\ r \end{bmatrix} \quad \ldots(5)$$

$$\mathbf{I} \begin{bmatrix} \dot{p} \\ \dot{q} \\ \dot{r} \end{bmatrix} + \begin{bmatrix} p \\ q \\ r \end{bmatrix} \times \left(\mathbf{I} \begin{bmatrix} p \\ q \\ r \end{bmatrix} \right) = \mathbf{m}, \quad \mathbf{I} = \begin{bmatrix} I_x & 0 & -I_{xz} \\ 0 & I_y & 0 \\ -I_{xz} & 0 & I_z \end{bmatrix} \quad \ldots(6)$$

$$\mathbf{m} = \begin{bmatrix} M_x \\ M_y \\ M_z \end{bmatrix} = \begin{bmatrix} I_x\dot{p} - I_{xz}\dot{r} \\ I_y\dot{q} \\ I_z\dot{r} - I_{xz}\dot{p} \end{bmatrix} + \begin{bmatrix} (I_z - I_y)qr - I_{xz}pq \\ (I_x - I_z)pr + (p^2 - r^2)I_{xz} \\ (I_y - I_x)pr + I_{xz}qr \end{bmatrix} \quad \ldots(7)$$

https://doi.org/10.1017/aer.2018.99 Published online by Cambridge University Press

The aerodynamic forces and moments defined in the wind axes are estimated using the component build-up approach in (8). The stability and control derivatives for the corresponding force and moment coefficients are used for this purpose:

$$\begin{aligned}
C_D &= \frac{D}{QS} = C_{D0} + C_{D1}C_L + C_{D2}C_L^2 + C_{D\delta_f}\,|\delta_f| \;+ C_{D\delta_a}\;|\delta_a| \;+ C_{D\delta_e}\;|\delta_e| \;+ C_{D\delta_r}\;|\delta_r| \\
C_\Upsilon &= \frac{\Upsilon}{QS} = C_{\Upsilon\beta}\beta + C_{\Upsilon p}\frac{pb}{2V_T} + C_{\Upsilon r}\frac{rb}{2V_T} + C_{\Upsilon\delta_a}\delta_a + C_{\Upsilon\delta_r}\delta_r \\
C_L &= \frac{L}{QS} = C_{L0} + C_{L\alpha}\alpha + C_{Lq}\frac{qc}{2V_T} + C_{L\delta_f}\delta_f + C_{L\delta_e}\delta_e \\
C_l &= \frac{\mathcal{L}}{QSb} = C_{l\beta}\beta + C_{lp}\frac{pb}{2V_T} + C_{lr}\frac{rb}{2V_T} + C_{l\delta_a}\delta_a + C_{l\delta_r}\delta_r \\
C_m &= \frac{\mathcal{M}}{QSc} = C_{m0} + C_{m\alpha}\alpha + C_{mq}\frac{qc}{2V_T} + C_{m\delta_f}\delta_f + C_{m\delta_e}\delta_e \\
C_n &= \frac{\mathcal{N}}{QSb} = C_{n\beta}\beta + C_{np}\frac{pb}{2V_T} + C_{nr}\frac{rb}{2V_T} + C_{n\delta_a}\delta_a + C_{n\delta_r}\delta_r
\end{aligned} \qquad \ldots(8)$$

The wind axes are obtained by rotating the body axes through α followed by β. The aerodynamic forces and moments defined in the wind axes can be related to the body axes force **f** and moment **m** by appropriate transformation as shown in (9) and (10). It is assumed that the aircraft flies in a co-ordinated fashion i.e. the side-slip β is negligible ($C_\beta \approx 1$ and $S_\beta \approx 0$). This assumption translates to imposing inequality constraints on β during optimisation (Table 2):

$$\mathbf{f} = \begin{bmatrix} F_x \\ F_y \\ F_z \end{bmatrix} = QS \begin{bmatrix} -C_\alpha C_D + S_\alpha C_L + C_{Tx} \\ C_\Upsilon + C_{Ty} \\ -S_\alpha C_D - C_\alpha C_L \end{bmatrix} \qquad \ldots(9)$$

$$\mathbf{m} = \begin{bmatrix} M_x \\ M_y \\ M_z \end{bmatrix} = QS \begin{bmatrix} bC_\alpha C_l - bS_\alpha C_n \\ cC_m \\ bS_\alpha C_l + bC_\alpha C_n + dC_{Ty} \end{bmatrix} \qquad \ldots(10)$$

Table 2
Constraints

Variable	Lower bound	Upper bound
x, y (m)	−500	500
z (m)	−100	$-\frac{1}{2}b\;\lvert\sin(\phi)\rvert$
V_T (m/s)	10	80
Load factor, n	−2	2
α (°)	−12	12
β (°)	−1	1
C_L	−0.2	1.17
ϕ (°)	−60	60
θ (°)	−60	60
δ_f, δ_a, δ_e, δ_r (°)	−30	30
C_{Tx}, C_{Ty}	-10^{-4}	10^{-4}
t_f (s)	0	100
V_R (m/s)	0	100
$\mathbf{b}_0$, $\mathbf{b}_{ci}$, $\mathbf{b}_{si}$	$-500[111111]T$	$500[111111]^T$
d (loiter)	$-4\pi[000001]T$	$4\pi[000001]^T$

https://doi.org/10.1017/aer.2018.99 Published online by Cambridge University Press

In (9) and (10), C_{Tx} and C_{Ty} denote the components of the normalised thrust along the body x- and y-axes, respectively. The propeller is placed at a distance d away from the CG along the body x-axis. This leads to a contribution from C_{Ty} to the moment along the body z-axis.

The set of 12 differential equations ((2), (3), (5) and (7)) for the 12 states – x, y, z, u, v, w, ϕ, θ, ψ, p, q, r constitute the aircraft's six-degree-of-freedom (6DoF) equations of motion involving 6 control inputs – δ_f, δ_a, δ_e, δ_r, C_{Tx}, C_{Ty}.

4.0 FLATNESS OF 6DoF AIRCRAFT

A dynamical system $\dot{\mathbf{x}} = \mathbf{g}(\mathbf{x},\mathbf{u})$ with state vector $\mathbf{x} \in \mathbb{R}^i$, input vector $\mathbf{u} \in \mathbb{R}^j$ and with a smooth vector field $\mathbf{g}$, is differentially flat[25] if there exists $\mathbf{y} \in \mathbb{R}^j$ of the form

$$\mathbf{y} = \mathbf{h}(\mathbf{x}, \mathbf{u}, \dot{\mathbf{u}}, \ \dots \ , \mathbf{u}^{(k)}) \qquad ...(11)$$

such that

$$\begin{aligned} &\mathbf{x} = \boldsymbol{\zeta}(\mathbf{y}, \dot{\mathbf{y}}, \ \dots \ , \mathbf{y}^{(k-1)}) \text{ and} \\ &\mathbf{u} = \boldsymbol{\xi}(\mathbf{y}, \dot{\mathbf{y}}, \ \dots \ , \mathbf{y}^{(k-1)}, \mathbf{y}^{(k)}) \end{aligned} \qquad ...(12)$$

where $\mathbf{h}$, $\boldsymbol{\zeta}$ and $\boldsymbol{\xi}$ are smooth vector fields defined as

$$\begin{aligned} &\mathbf{h} : \mathbb{R}^i \times (\mathbb{R}^j)^{k+1} \rightarrow \mathbb{R}^j, \\ &\boldsymbol{\zeta} : (\mathbb{R}^j)^k \rightarrow \mathbb{R}^i \text{ and} \\ &\boldsymbol{\xi} : (\mathbb{R}^j)^{k+1} \rightarrow \mathbb{R}^j \end{aligned} \qquad ...(13)$$

From (12), it is seen that all the states and the control inputs can be expressed in terms of the flat outputs and their time derivatives. In addition, there must not exist any differential relation of the form $\mathbf{r}(\mathbf{y}, \dot{\mathbf{y}}, \ldots, \mathbf{y}^{(\kappa)}) = 0$ i.e. the flat outputs $\mathbf{y}$ should be differentially independent.

The system of 12 nonlinear differential equations described in the previous section will be shown to be differentially flat. The aircraft's inertial frame co-ordinates and the body axes Euler angles, (x, y, z, ϕ, θ, ψ), are picked as flat outputs. All the states and the control inputs can be uniquely represented in terms of these flat outputs and their first two derivatives. Furthermore, the flat outputs are solely a function of the states. In such cases, the system is said to be 0-flat. By rearranging (2) and (5), the states (u, v, w, p, q, r) and their first derivatives can be expressed in terms of the flat outputs as shown in (A.5) and (A.6). These are then substituted into (4) and (7) to obtain $\mathbf{f}$ and $\mathbf{m}$, respectively. Following this, (8) is plugged into (9) and (10) to obtain the solution for the control inputs. As a consequence of assuming the side-slip to be negligible, the lateral and the longitudinal aerodynamics become decoupled. This means that the solution to δ_f, δ_e and C_{Tx} can be obtained independently of δ_a, δ_r and C_{Ty}. The important steps involved are summarised below.

https://doi.org/10.1017/aer.2018.99 Published online by Cambridge University Press

4.1 Solution for δ_f, δ_e, C_{Tx}

The terms involving the absolute values of the control inputs are dropped from the expression of C_D in (8) in order to make the process of evaluating the control inputs tractable. This inconsistency is accounted for by adding an extra term $\tilde{C}_{D0}$, given by (14), to the drag coefficient. It corresponds to the drag incurred due to average control surface deflections during the period of flight. The x and z components of the body axes force $\mathbf{f}$ in (9) can be rearranged to yield (15):

$$\tilde{C}_{D0} = C_{D\delta_f} \left|\delta_f\right|_{\text{avg.}} + C_{D\delta_a} \left|\delta_a\right|_{\text{avg.}} + C_{D\delta_e} \left|\delta_e\right|_{\text{avg.}} + C_{D\delta_r} \left|\delta_r\right|_{\text{avg.}} \quad ...(14)$$

$$\begin{aligned} f_1 &= \frac{F_x}{QS} S_\alpha - \frac{F_z}{QS} C_\alpha = C_L + S_\alpha C_{Tx} \\ f_2 &= \frac{F_x}{QS} C_\alpha + \frac{F_z}{QS} S_\alpha = -C_D + C_\alpha C_{Tx} \end{aligned} \quad ...(15)$$

$$C_D = a_0 + a_1 C_L + a_2 C_L^2, \quad \begin{aligned} a_0 &= C_{D0} + \tilde{C}_{D0} \\ a_1 &= C_{D1} \\ a_2 &= C_{D2} \end{aligned} \quad ...(16)$$

A quadratic equation (17) for C_{Tx} can be obtained from (15) and (16):

$$(a_2 S_\alpha^2) C_{Tx}^2 + (-a_1 S_\alpha - 2a_2 f_1 S_\alpha - C_\alpha) C_{Tx} + (a_0 + a_1 f_1 + a_2 f_1^2 + f_2) = 0 \quad ...(17)$$

The constants f_1, f_2, a_0, a_1 and a_2 are introduced merely for convenience in notation. A simple order of magnitude analysis (A.7–A.10) reveals that only one of the solutions of (17) is physically realisable, hence leaving no room for ambiguity:

$$C_{Tx} = \left(\frac{a_1 S_\alpha + 2a_2 f_1 S_\alpha + C_\alpha}{2a_2 S_\alpha^2}\right) - \sqrt{\left(\frac{a_1 S_\alpha + 2a_2 f_1 S_\alpha + C_\alpha}{2a_2 S_\alpha^2}\right)^2 - \left(\frac{a_0 + a_1 f_1 + a_2 f_1^2 + f_2}{a_2 S_\alpha^2}\right)} \quad ...(18)$$

C_L is determined by plugging this solution for C_{Tx} into (15) while C_m is known from (10). Two linear equations in δ_f and δ_e are then obtained using the expansions for C_L and C_m in (8):

$$\begin{aligned} \frac{M_y}{QSc} &= \overbrace{\left(C_{m0} + C_{m\alpha}\alpha + C_{mq}\left(\frac{qc}{2V_T}\right)\right)}^{a_m} + \overbrace{\begin{bmatrix} C_{m\delta_f} & C_{m\delta_e} \end{bmatrix}}^{\mathbf{a}_m} \begin{bmatrix} \delta_f \\ \delta_e \end{bmatrix} \\ C_L = f_1 - S_\alpha C_{Tx} &= \overbrace{\left(C_{L0} + C_{L\alpha}\alpha + C_{Lq}\left(\frac{qc}{2V_T}\right)\right)}^{a_L} + \overbrace{\begin{bmatrix} C_{L\delta_f} & C_{L\delta_e} \end{bmatrix}}^{\mathbf{a}_L} \begin{bmatrix} \delta_f \\ \delta_e \end{bmatrix} \end{aligned} \quad ...(19)$$

$$\begin{bmatrix} \frac{M_y}{QSc} - a_m \\ f_1 - S_\alpha C_{Tx} - a_L \end{bmatrix} = \begin{bmatrix} \mathbf{a}_m \\ \mathbf{a}_L \end{bmatrix} \begin{bmatrix} \delta_f \\ \delta_e \end{bmatrix} \quad ...(20)$$

https://doi.org/10.1017/aer.2018.99 Published online by Cambridge University Press

4.2 Solution for δ_a, δ_r, C_{Ty}

The expansions for C_Υ, C_l and C_n from (8) are substituted into the expressions for F_y, M_x and M_z in (9) and (10). A system of three linear equations in δ_a, δ_r and C_{Ty} is obtained:

$$
\begin{aligned}
C_l &= \overbrace{\left(C_{l\beta}\beta + C_{lp}\left(\frac{pb}{2V_T}\right) + C_{lr}\left(\frac{rb}{2V_T}\right)\right)}^{a_l} + \overbrace{\begin{bmatrix} C_{l\delta_a} & C_{l\delta_r} & 0 \end{bmatrix}}^{\mathbf{a}_l} \begin{bmatrix} \delta_a \\ \delta_r \\ C_{Ty} \end{bmatrix} \\
C_n &= \overbrace{\left(C_{n\beta}\beta + C_{np}\left(\frac{pb}{2V_T}\right) + C_{nr}\left(\frac{rb}{2V_T}\right)\right)}^{a_n} + \overbrace{\begin{bmatrix} C_{n\delta_a} & C_{n\delta_r} & 0 \end{bmatrix}}^{\mathbf{a}_n} \begin{bmatrix} \delta_a \\ \delta_r \\ C_{Ty} \end{bmatrix} \\
\frac{F_y}{QS} &= \overbrace{\left(C_{\Upsilon\beta}\beta + C_{\Upsilon p}\left(\frac{pb}{2V_T}\right) + C_{\Upsilon r}\left(\frac{rb}{2V_T}\right)\right)}^{a_\Upsilon} + \overbrace{\begin{bmatrix} C_{\Upsilon\delta_a} & C_{\Upsilon\delta_r} & 0 \end{bmatrix}}^{\mathbf{a}_\Upsilon} \begin{bmatrix} \delta_a \\ \delta_r \\ C_{Ty} \end{bmatrix} \\
&\quad + \overbrace{\begin{bmatrix} 0 & 0 & 1 \end{bmatrix}}^{\mathbf{a}_t} \begin{bmatrix} \delta_a \\ \delta_r \\ C_{Ty} \end{bmatrix}
\end{aligned}
\qquad \ldots(21)
$$

Collecting (21) into a compact form yields us the following equation:

$$
\begin{bmatrix} \frac{M_x}{QSb} - (C_\alpha a_l - S_\alpha a_n) \\ \frac{M_z}{QSb} - (S_\alpha a_l + C_\alpha a_n) \\ \frac{F_y}{QS} - a_\Upsilon \end{bmatrix} = \begin{bmatrix} C_\alpha \mathbf{a}_l - S_\alpha \mathbf{a}_n \\ S_\alpha \mathbf{a}_l + C_\alpha \mathbf{a}_n + \frac{d}{b}\mathbf{a}_t \\ \mathbf{a}_\Upsilon + \mathbf{a}_t \end{bmatrix} \begin{bmatrix} \delta_a \\ \delta_r \\ C_{Ty} \end{bmatrix} \qquad \ldots(22)
$$

The flatness of a 6DoF aircraft model with conventional control surfaces and thrust vectoring ability has been brought out. The next section demonstrates how this can be effectively applied to trajectory optimisation for dynamic soaring.

5.0 TRAJECTORY OPTIMISATION FOR DYNAMIC SOARING

The proposed recipe of flatness is applied to 6DoF dynamic soaring trajectory optimisation. As mentioned earlier, dynamic soaring involves the extraction of energy from wind gradient for sustained un-powered flight. Given an aircraft model, it is desirable to know the limiting condition under which it can exhibit dynamic soaring. This corresponds to determining the minimum strength of wind gradient required for achieving the same. In the wind model (2) that is considered in this work, the magnitude of reference wind speed V_R quantifies the strength of wind gradient. The objective of the trajectory optimisation problem is, therefore, the minimisation of V_R. Trajectories where the chosen aircraft can exhibit dynamic soaring with the aid of as low a wind gradient strength as possible are sought.

All the 12 states and the six control inputs have been expressed in terms of the six flat outputs. The dimension of the system is effectively halved and the problem of trajectory optimisation is confined to the space of the flat outputs. The trajectories associated with dynamic soaring necessitate all or most of the states to be periodic. It is then apt to consider a

https://doi.org/10.1017/aer.2018.99 Published online by Cambridge University Press

Fourier series-like representation for the flat outputs, $\mathbf{y} = [x\ y\ z\ \phi\ \theta\ \psi]^T$, given by (23), where M is the number of harmonics:

$$\mathbf{y} = \mathbf{d}\frac{t}{t_f} + \mathbf{b}_0 + \sum_{i=1}^{M}\left\{\mathbf{b}_{ci}\cos\left(2\pi i\frac{t}{t_f}\right) + \mathbf{b}_{si}\sin\left(2\pi i\frac{t}{t_f}\right)\right\} \quad ...(23)$$

In (23), t_f represents the time-period of the trajectory and the linear term $\mathbf{d}$ is incorporated to model travelling trajectories[7]. The elements corresponding to ϕ, θ and z in $\mathbf{d}$ are set to zero as these states are necessarily periodic for all kinds of energy-neutral trajectories. The Fourier coefficients of the flat outputs, period of flight t_f and the reference wind speed V_R are treated as the design variables. All of these are collected into the design vector $\mathbf{z}$:

$$\mathbf{z} = \begin{bmatrix}\mathbf{d}^T & \mathbf{b}_0^T & \mathbf{b}_{c1}^T & \mathbf{b}_{s1}^T & \cdots & \mathbf{b}_{cM}^T & \mathbf{b}_{sM}^T & t_f & V_R\end{bmatrix}^T \quad ...(24)$$

The optimisation problem is stated as follows:

$$\begin{array}{ll}\text{minimise} & V_R \\ \text{such that} & \mathbf{l}_b \le \mathbf{z} \le \mathbf{u}_b \\ & \mathbf{c}(\mathbf{z}) \le 0\end{array} \quad ...(25)$$

Even though all the states and the controls can be derived from the flat outputs, all combinations for these flat outputs would not translate to physically realisable values for states and controls. For this reason, inequality constraints $\mathbf{c}(\mathbf{z})$ are imposed at N uniformly spaced points within the period. In addition to this, upper bound $\mathbf{u}_b$ and lower bound $\mathbf{l}_b$ are imposed on $\mathbf{z}$. Table 2 lists the constrained variables and their bounds. In order to obtain closed or cross-country trajectories, appropriate constraints are placed on the elements of $\mathbf{d}$ corresponding to x and y. The thrust inputs along both the axes are constrained to lie close to zero as the primary motive behind dynamic soaring is to illustrate sustained flight without expending energy from the power plant.

5.1 Initial guess

A proper initial guess is necessary for the optimiser to yield a converged solution to the proposed optimisation problem within a reasonable time. It is observed that the solution to the 3DoF flatness-based trajectory optimisation serves as a good initial guess for the proposed 6DoF version. The 3DoF (point mass) version has been implemented by Deittert et al.[7], where the inertial frame co-ordinates of the aircraft (x, y, z) are treated as flat outputs. The coefficients of the Fourier series representation of these outputs serve as design variables. It is noted that the solver consistently fails to converge when an arbitrary initial guess, consisting of pseudo-random values or zeros is provided. On the other hand, provision of initial guesses that capture the approximate shape of the sought dynamic soaring trajectory ensures near-certain convergence of the optimiser. Guess trajectories that mimic the "O" and "∞" shaped dynamic soaring trajectories are shown in Table 3. A Fourier series representation of these is provided as an initial guess to the optimiser. A similar approach was followed in Liu et al.[23], although the optimisation was performed in time-domain. Cross-country or travelling trajectories can be obtained using the same initial guesses as that for the closed orbits but with constraints placed on the appropriate elements of $\mathbf{d}$. Once the optimal solution for the flat

https://doi.org/10.1017/aer.2018.99 Published online by Cambridge University Press

Table 3
Initial guess for 3DoF implementation

	"O" shape	"∞" shape
x	$20\left(-1+\cos\left(2\pi t/t_f\right)\right)$	$-20\ \sin\ \left(4\pi t/t_f\right)$
y	$-20\sqrt{2}\ \sin\ \left(2\pi t/t_f\right)$	$-40\sqrt{2}\ \sin\ \left(2\pi t/t_f\right)$
z	$-20\left(1-\cos\left(2\pi t/t_f\right)\right)$	$-20\left(\sin\ \left(4\pi t/t_f\right)+1\right)$

outputs of the 3DoF implementation is obtained, the wind axes orientation angles can be computed by invoking the property of flatness. The details are provided in Deittert et al.[7]. These angles serve as a good approximation for the Euler angles of the 6DoF aircraft when α and β are small. The Fourier series approximation for the position time-history and, for these wind axes orientation angles are then provided as initial guess for the 6DoF implementation. Furthermore, the stability and the control derivatives that are required in (8) are estimated for trimmed flight at the mean airspeed observed in the 3DoF solution. This effectively means that the proposed method requires a carefully selected initial guess for the position time-trajectory alone to initiate the flatness-based 3DoF optimisation, whose solution subsequently kick-starts the proposed flatness-based 6DoF optimisation.

5.2 Results

The optimisation problem is solved in MATLAB® using the nonlinear programming solver, fmincon, and within that the Interior-Point algorithm is selected. The solution for closed and travelling trajectories along with the attitude of the aircraft are illustrated in Figs 6 and 7. The 3DoF trajectories which are provided as initial guesses are also indicated. The optimal wind field strength V_R and the period t_f of the various trajectory solutions are given in Table 4. The observation that the wind strength required for making upwind progress is considerably higher than that required to make the same amount of downwind progress subscribes to the expectations. Among the closed (loiter) trajectories, the "∞" shape requires a smaller wind strength than the "O" shape. Liu et al.[23] have also arrived at the same conclusion and the optimal V_R and t_f calculated by them are very close to that obtained in the present work. The small discrepancy observed is due to the difference in the aircraft models considered. The optimality of the "∞" shape over the "O" shape comes at the cost of large variations in the angle of attack and the control surface deflections (Fig. 4).

It is seen that the side-slip and the thrust inputs (Figs 3(b) and (d) and 4(b) and (d)) lie within the bounds prescribed in Table 2. Moreover, the assumption of quasi-steady flow

Table 4
Optimal parameters

Trajectory	V_R (m/s)	t_f (s)
"O" shape	8.74	16.40
"∞" shape	6.96	26.84
Downwind travel	7.45	13.14
Upwind travel	13.58	26.43

https://doi.org/10.1017/aer.2018.99 Published online by Cambridge University Press

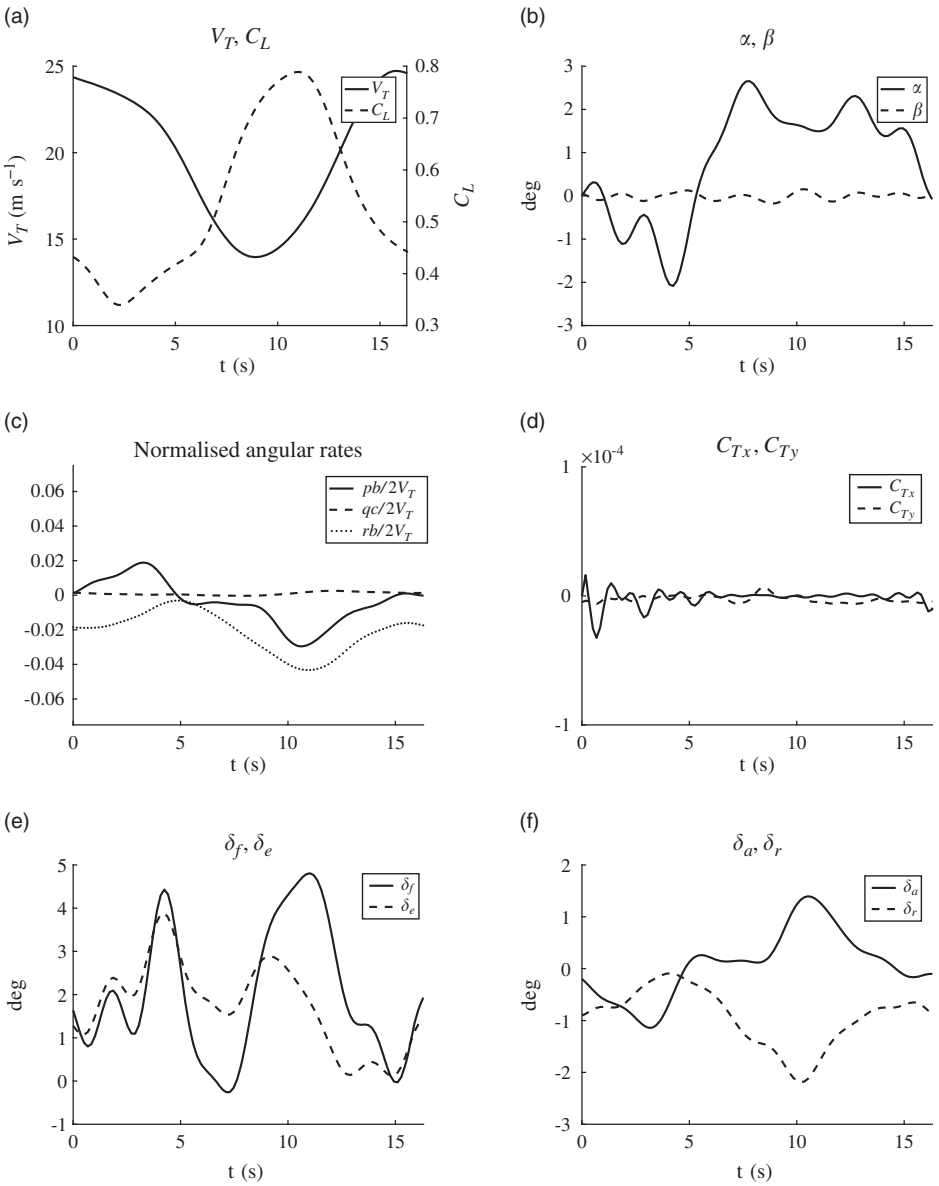


Figure 3. "O" trajectory.

inherent in the aerodynamic model is justified as the normalised angular velocity components (Figs 3(c) and 4(c)) are well within the bounds[22] where the reduced frequency is low.

The optimal trajectory solutions from the proposed method are obtained with an approximation (14) introduced to the expression of C_D. Furthermore, since the optimal thrust inputs take very small values within the prescribed bounds, they can be considered to be zero from a practical standpoint. Even after these approximations are accounted for, the optimal solution for the control surface deflections obtained from the proposed flatness-based optimisation is

https://doi.org/10.1017/aer.2018.99 Published online by Cambridge University Press

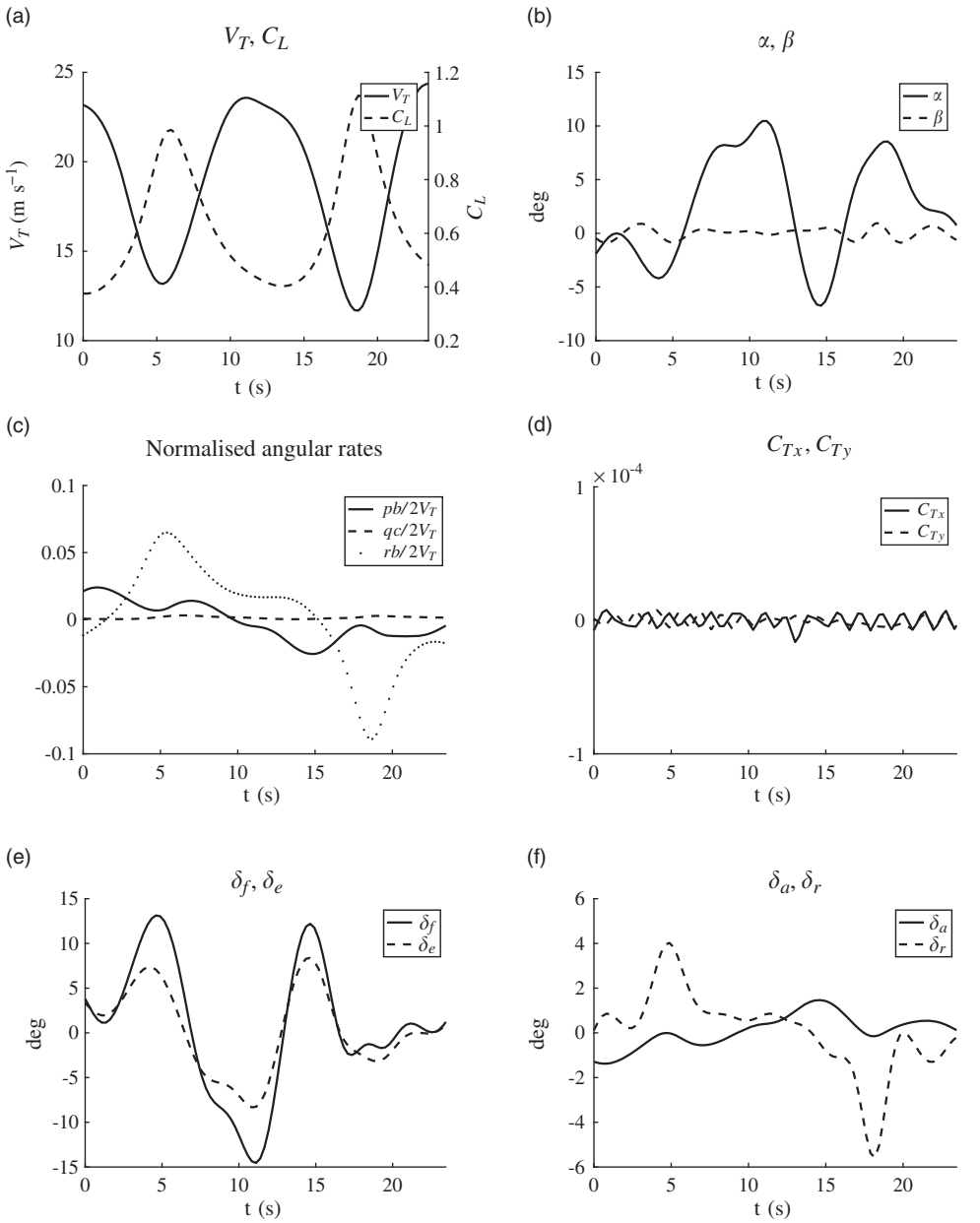


Figure 4. "∞" trajectory.

seen to give satisfactory results. The aircraft equations of motion containing the higher fidelity expression for C_D in (8) are time-marched with the optimal control surface deflections and with the thrust inputs set to zero (Fig. 5). It is observed that the error (RMSE) between the time-marched trajectory and that obtained from optimisation does not exceed 0.5 m for "O" shape, and 4 m for "∞" shape. Given the scale of these trajectories, this amounts to less than 5% error. The presence of different time-scales in the aircraft dynamics can be observed in the

https://doi.org/10.1017/aer.2018.99 Published online by Cambridge University Press

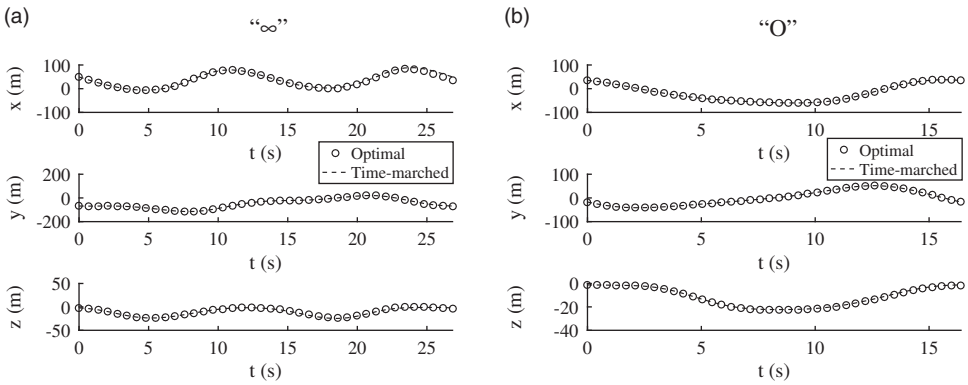


Figure 5. Optimal trajectory and time-marched trajectory

obtained trajectory solutions (Figs 3 and 4). The contribution of higher harmonics is more evident in the control surface time-histories. The position time-history, on the other hand, does not show rapid variations i.e. the contribution of lower harmonics is dominant. The relative magnitude of the coefficients in their Fourier series representation verifies this observation.

The optimal wind gradient strength reduces when the number of harmonics in the Fourier series expansion of the flat outputs is increased. However, no significant improvement in the optimal solution is noted when more than 12 harmonics are considered.

Visual inspection of the aircraft's attitude near the top portion of the trajectories, especially in Figs 6(b) and 7(a), seems to indicate a considerably large side-slip. This is in apparent conflict with the computed optimal time-history of β (Figs 3(b) and 4(b)) where the prescribed bounds are not seen to be violated. This apparent discrepancy can be resolved by noting that near the top portion of the trajectory, there is a considerable difference between the aircraft's airspeed and its inertial frame speed. The large side-slip that is observed in the plots is between the body axes and the inertial frame velocity. On the contrary, the true side-slip β between the body axes and the relative wind vector is indeed small as indicated in Figs 3(b) and 4(b).

5.2.1 Comparison with the collocation-based optimisation

A direct collocation-based trajectory optimisation is compared with the proposed flatness-based implementation. The former is implemented using Chebyshev pseudospectral method where the set of 12 differential equations are discretized using the Chebyshev differentiation matrix and are posed as nonlinear algebraic equality constraints. These constraints are imposed on a grid of points with Chebyshev spacing within the period of flight. In addition to this, constraints on control rates and those given in Table 2 are also imposed. Chebyshev spacing clusters the grid points towards the extremities and leaves the middle sparse. Due to this, it is observed that at least 35–40 points are required to obtain a satisfactory trajectory solution. The details of the method are provided in Fahroo and Ross[26]. The advantage of the flatness-based optimisation is multi-fold. The dimensionality of the direct collocation-based optimisation is significantly higher than that of the proposed flatness-based method. For a trajectory parameterised with 40 points, the former involves 722 design variables while the latter only has 132 when a ten-harmonic representation for the flat outputs is used. The comparison of the trajectory solutions obtained for a linear wind field ($\mathfrak{p} = 1$) from the two

https://doi.org/10.1017/aer.2018.99 Published online by Cambridge University Press

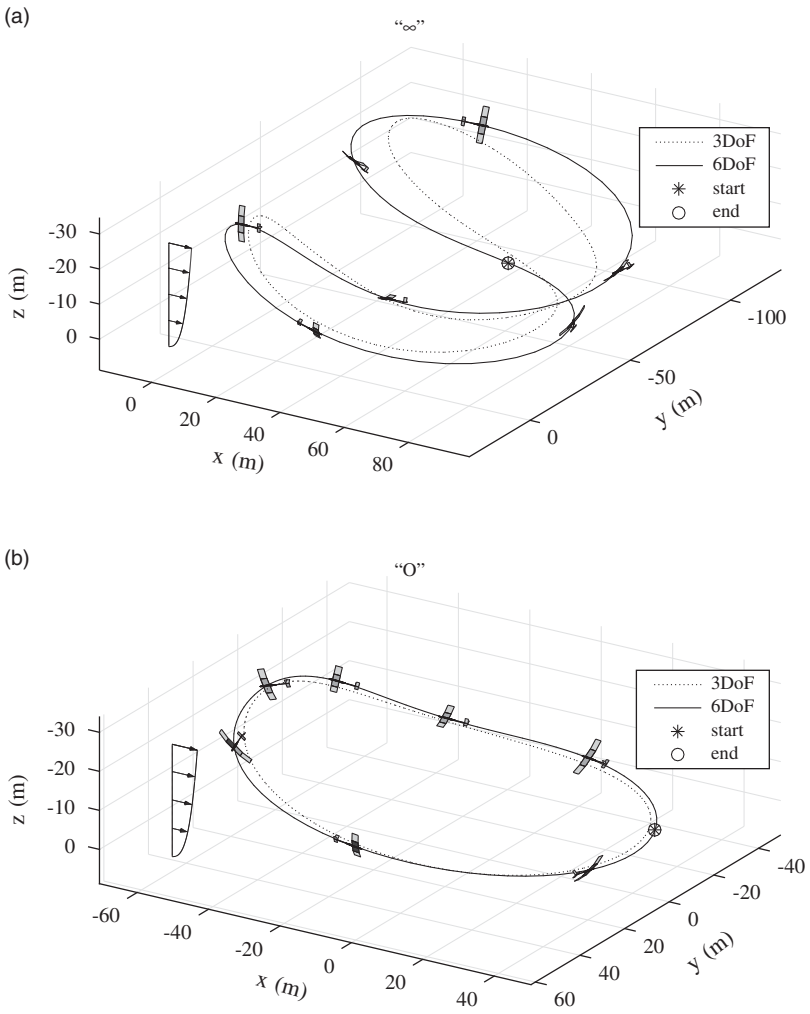


Figure 6. Closed trajectories.

approaches is shown in Fig. 8 and Table 5. The codes are run on a machine with 4th generation Intel® CORE™ i7 2.6 GHz processor and 8GB of RAM. The flatness-based method has a considerably smaller computational time and yields a continuous solution as compared to the discrete trajectory obtained from the collocation approach. Also, the slightly larger value of V_R from the former should not be construed as the sub-optimality of the flatness-based method over the collocation approach. Such a conclusion cannot be drawn unless a convergence study based on the number of harmonics, collocation points and over a range of initial guesses is undertaken. Second, the control time-histories obtained from the proposed flatness-based implementation are near-optimal but smooth because the flat outputs are parameterised with infinitely differentiable basis functions. On the other hand, the collocation method yields control solutions that possess rapid fluctuations. These fluctuations can be eliminated with the scaling of the control inputs to the same order of magnitude and with the inclusion of constraints on their first derivatives. Another disadvantage that the collocation method suffers from is the inability to converge in a single attempt with the

https://doi.org/10.1017/aer.2018.99 Published online by Cambridge University Press

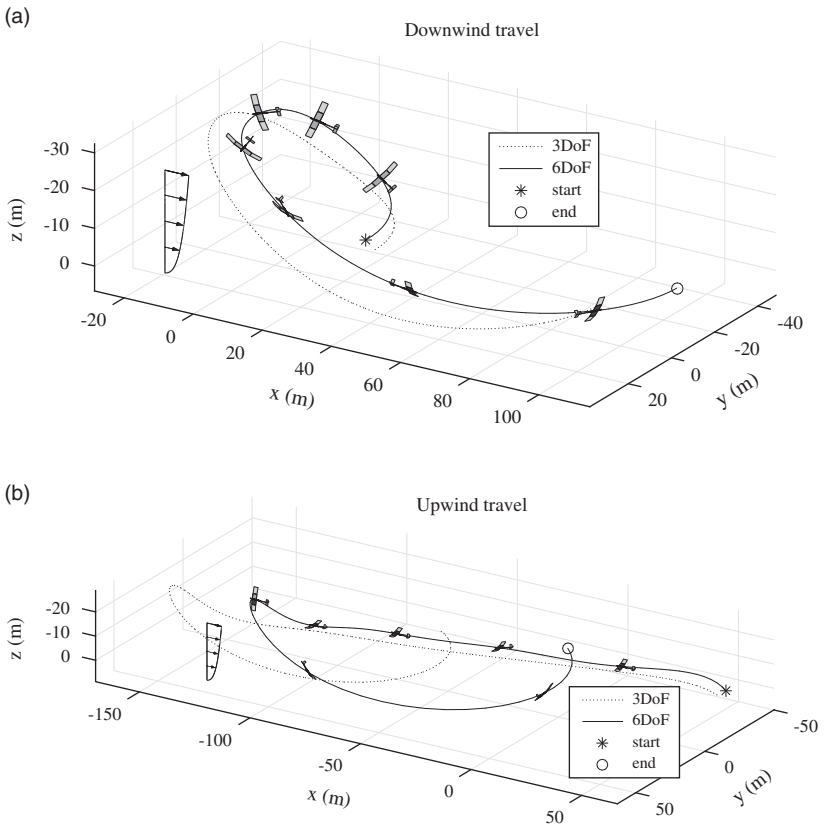


Figure 7. Travelling trajectories.

prescribed initial guess (Table 3) when the wind field is changed from linear to exponential. In order to obtain a converged solution for $\mathfrak{p} = 0.25$, solutions need to be obtained for higher values of $\mathfrak{p}$ (<1) in descending order and used as an initial guess for the optimiser successively. The flatness method, on the contrary, obtains a converged solution in a single attempt without the need for any iterations.

At this conjecture, it is apposite to take note of certain salient features and limitations of the proposed recipe of 6DoF aircraft flatness. The provision of six control inputs in an aircraft model, as described in Section 3, is necessary for the proposed recipe to be viable. That being said, for applications involving trajectory generation or tracking, the absent control inputs can be constrained to lie near zero during optimisation. Their contribution, as a consequence, is made negligible, which is equivalent to their absence. This has been demonstrated in the present trajectory optimisation problem where the thrust inputs are constrained (Figs 3(d) and 4(d)). The aerodynamics model is obtained through linearisation about a reference state (steady level cruise). Such a model is valid for trajectories that do not significantly deviate from the reference state. Furthermore, the linear aerodynamics model yields quasi-steady estimate of the forces and moments. In order for the quasi-steady estimate to be reliable, the reduced frequency associated with the flight manoeuvre must be sufficiently small and the angle of attack must not venture into the stall regime. The bounds on the normalised body angular rates suggested by Drela and Youngren[22] demarcate the region where the

https://doi.org/10.1017/aer.2018.99 Published online by Cambridge University Press

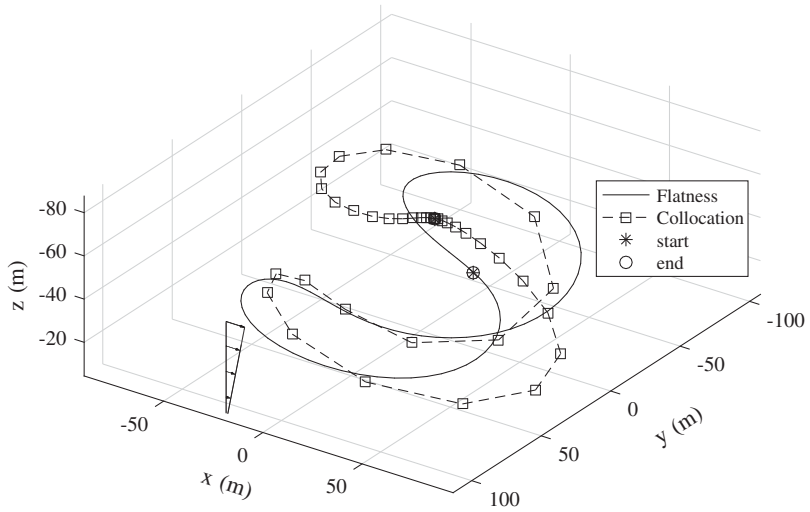


Figure 8. "∞" trajectories from collocation and flatness methods.

Table 5
"∞" trajectory from flatness and collocation-based optimisation

Method	V_R (m/s)	Solution time (s)	Design variables
Flatness	0.178	175	132
Collocation (40 points)	0.151	709	722

quasi-steady assumption is valid. Another crucial assumption that the proposed recipe relies on is that of co-ordinated flight ($\beta \approx 0$). Except in aero-acrobatic manoeuvres, it is usually desirable that the aircraft flies in a co-ordinated fashion. When the side-slip is small, the proposed recipe holds, which as a result allows the aircraft trajectories to be planned in the flat output space. Constraints can be imposed during optimisation such that β lies in a small band near zero, as seen in Figs 3(b) and 4(b).

Aggressive flight manoeuvres are typically costly, in the sense that the airframe is subjected to larger loads and higher fuel consumption is necessitated. In applications involving trajectory generation for reconnaissance or station-keeping missions, it is usually preferable to restrict to benign manoeuvres. The proposed recipe could be advantageous for generating non-aggressive trajectories where α and β are small, and the reduced frequency is sufficiently low. It has been illustrated that the optimal 3DoF solution of a trajectory optimisation problem can be used to construct a good initial guess for the related 6DoF problem, as described in Section 5.1. Furthermore, by using the 3DoF trajectory optimisation solution, an appropriate reference state for linearising the 6DoF aerodynamics can be inferred. The average airspeed over the duration of flight can be determined from the 3DoF solution. Steady level cruise at this mean airspeed would serve as an appropriate reference for linearisation, provided the minimum and the maximum airspeed encountered during the manoeuvre is not significantly different from the mean airspeed. Finally, the proposed recipe has made use of thrust vectoring capability that is confined to the x–y plane. Ideally, it would be more advantageous to vector thrust in all the directions.

https://doi.org/10.1017/aer.2018.99 Published online by Cambridge University Press

Martin's[14] formulation of flatness, in contrast, is applicable for a wider region in the flight envelope as it employs a look-up table spanning operating points for estimating the aerodynamic coefficients. However, the use of a look-up table for trajectory generation or tracking is computationally costly. For this reason, a slightly less accurate low-order functional form for the aircraft's aerodynamic coefficients (as shown in (8)) is preferable. In addition to this, the advantage of taking the aid of the optimal 3DoF solution to solve a 6DoF trajectory optimisation is absent from Martin's formulation.

6.0 CONCLUSION

This work illustrates the flatness of a 6DoF aircraft model with conventional control surfaces and applies it to dynamic soaring trajectory optimisation. The information about the aircraft's position and attitude time-history are sufficient to characterise all states and inputs of the aircraft. The proposed method has significant advantages over collocation-based optimisation, most importantly reduced computational cost, which makes it feasible for real-time applications.

It is crucial to provide an appropriate initial guess to ensure the success of the 6DoF flatness-based optimisation. In this regard, a connection can be observed between the 3DoF and the proposed 6DoF implementations. It is fairly easy to obtain a solution to the 3DoF optimisation starting with an intuitively selected initial guess for the position time-history (flat outputs in the 3DoF version). Using this solution, the wind axes orientation angles can be computed which are a good approximation for the Euler angles of the 6DoF aircraft when α and β are small. The Fourier series approximation for these angles and for the position trajectory serves as a good initial guess for the 6DoF flatness-based optimisation. Effectively, this means that guessing the aircraft's position trajectory alone is sufficient to obtain an optimal solution for all states and controls of the 6DoF aircraft in a reasonable time.

This initial guess from the 3DoF solution is not by itself satisfactory as the nonlinear constraints related to β and C_{Ty} (Table 2) are violated. This is expected because the 3DoF implementation ignores the lateral dynamics of the aircraft. Hence, optimisation is necessary.

Although the flatness of the 6DoF aircraft model requires the inclusion of six control inputs, it is important to note that the proposed method is also applicable for aircraft models which lack flap input and thrust vectoring ability. During optimisation, the absent control inputs can be constrained to remain close to zero, thereby negating their effect. This is precisely what has been done in the dynamic soaring problem where the thrust inputs are constrained to lie close to zero.

In a real-time implementation, the proposed method can be used to rapidly compute near-optimal solutions with lesser harmonics. The aircraft can engage in these low-order trajectories while more optimal higher order solutions are computed successively by using the low order solutions as initial guess.

APPENDIX

Miscellaneous expressions

$$\alpha = \arctan(w/u), \quad \beta = \arcsin(v/V_T)$$
$$V_T = \sqrt{u^2 + v^2 + w^2} \qquad \ldots(A.1)$$

https://doi.org/10.1017/aer.2018.99 Published online by Cambridge University Press

$$\mathbf{S} = \begin{bmatrix} C_\psi C_\theta & S_\psi C_\theta & -S_\theta \\ C_\psi S_\theta S_\phi - S_\psi C_\phi & S_\psi S_\theta S_\phi + C_\psi C_\phi & C_\theta S_\phi \\ C_\psi S_\theta C_\phi + S_\psi S_\phi & S_\psi S_\theta C_\phi - C_\psi S_\phi & C_\theta C_\phi \end{bmatrix} \quad \text{...(A.2)}$$

$$\boldsymbol{\varphi} = \mathbf{S}\begin{bmatrix} W_x \\ 0 \\ 0 \end{bmatrix} = \begin{bmatrix} W_x C_\psi C_\theta \\ W_x\left(C_\psi S_\theta S_\phi - S_\psi C_\phi\right) \\ W_x\left(C_\psi S_\theta C_\phi + S_\psi S_\phi\right) \end{bmatrix} \quad \text{...(A.3)}$$

$$\dot{\boldsymbol{\varphi}} = \begin{bmatrix} \dot{\varphi}_x \\ \dot{\varphi}_y \\ \dot{\varphi}_z \end{bmatrix} = \begin{bmatrix} W_x\left(-\dot{\psi}S_\psi C_\theta - \dot{\theta}C_\psi S_\theta\right) + W_{xz}\dot{z}C_\psi C_\theta \\ W_x\left(-\dot{\psi}S_\psi S_\theta S_\phi + \dot{\theta}C_\psi C_\theta S_\phi + \dot{\phi}C_\psi S_\theta C_\phi - \dot{\psi}C_\psi C_\phi + \dot{\phi}S_\psi S_\phi\right) + W_{xz}\dot{z}\left(C_\psi S_\theta S_\phi - S_\psi C_\phi\right) \\ W_x\left(-\dot{\psi}S_\psi S_\theta C_\phi + \dot{\theta}C_\psi C_\theta C_\phi - \dot{\phi}C_\psi S_\theta S_\phi + \dot{\psi}C_\psi S_\phi + \dot{\phi}S_\psi C_\phi\right) + W_{xz}\dot{z}\left(C_\psi S_\theta C_\phi + S_\psi S_\phi\right) \end{bmatrix} \quad \text{...(A.4)}$$

$$\begin{aligned}
u &= \dot{x}C_\psi C_\theta + \dot{y}S_\psi C_\theta - \dot{z}S_\theta - W_x C_\psi C_\theta \\
v &= \dot{x}\left(C_\psi S_\theta S_\phi - S_\psi C_\phi\right) + \dot{y}\left(S_\psi S_\theta S_\phi + C_\psi C_\phi\right) + \dot{z}C_\theta S_\phi - W_x\left(C_\psi S_\theta S_\phi - S_\psi C_\phi\right) \\
w &= \dot{x}\left(C_\psi S_\theta C_\phi + S_\psi S_\phi\right) + \dot{y}\left(S_\psi S_\theta C_\phi - C_\psi S_\phi\right) + \dot{z}C_\theta C_\phi - W_x\left(C_\psi S_\theta C_\phi + S_\psi S_\phi\right) \\
\dot{u} &= \ddot{x}C_\psi C_\theta - \dot{x}\dot{\psi}S_\psi C_\theta - \dot{x}\dot{\theta}C_\psi S_\theta + \ddot{y}S_\psi C_\theta + \dot{y}\dot{\psi}C_\psi C_\theta - \dot{y}\dot{\theta}S_\psi S_\theta - \ddot{z}S_\theta - \dot{z}\dot{\theta}C_\theta - \dot{\varphi}_x \\
\dot{v} &= \ddot{x}\left(C_\psi S_\theta S_\phi - S_\psi C_\phi\right) + \dot{x}\left(-\dot{\psi}S_\psi S_\theta S_\phi + \dot{\theta}C_\psi C_\theta S_\phi + \dot{\phi}C_\psi S_\theta C_\phi - \dot{\psi}C_\psi C_\phi + \dot{\phi}S_\psi S_\phi\right) \\
&\quad + \ddot{y}\left(S_\psi S_\theta S_\phi + C_\psi C_\phi\right) + \dot{y}\left(\dot{\psi}C_\psi S_\theta S_\phi + \dot{\theta}S_\psi C_\theta S_\phi + \dot{\phi}S_\psi S_\theta C_\phi - \dot{\psi}S_\psi C_\phi - \dot{\phi}C_\psi S_\phi\right) \\
&\quad + \ddot{z}C_\theta S_\phi - \dot{z}\dot{\theta}S_\theta S_\phi + \dot{z}\dot{\phi}C_\theta C_\phi - \dot{\varphi}_y \\
\dot{w} &= \ddot{x}\left(C_\psi S_\theta C_\phi + S_\psi S_\phi\right) + \dot{x}\left(-\dot{\psi}S_\psi S_\theta C_\phi + \dot{\theta}C_\psi C_\theta C_\phi - \dot{\phi}C_\psi S_\theta S_\phi + \dot{\psi}C_\psi S_\phi + \dot{\phi}S_\psi C_\phi\right) \\
&\quad + \ddot{y}\left(S_\psi S_\theta C_\phi - C_\psi S_\phi\right) + \dot{y}\left(\dot{\psi}C_\psi S_\theta C_\phi + \dot{\theta}S_\psi C_\theta C_\phi - \dot{\phi}S_\psi S_\theta S_\phi + \dot{\psi}S_\psi S_\phi - \dot{\phi}C_\psi C_\phi\right) \\
&\quad + \ddot{z}C_\theta C_\phi - \dot{z}\dot{\theta}S_\theta C_\phi - \dot{z}\dot{\phi}C_\theta S_\phi - \dot{\varphi}_z
\end{aligned} \quad \text{...(A.5)}$$

$$\begin{aligned}
p &= \dot{\phi} - \dot{\psi}S_\theta \\
q &= \dot{\theta}C_\phi + \dot{\psi}C_\theta S_\phi \\
r &= -\dot{\theta}S_\phi + \dot{\psi}C_\theta C_\phi \\
\dot{p} &= \ddot{\phi} - \dot{\theta}\dot{\psi}C_\theta - \ddot{\psi}S_\theta \\
\dot{q} &= \ddot{\theta}C_\phi - \dot{\theta}\dot{\phi}S_\phi + \ddot{\psi}C_\theta S_\phi - \dot{\psi}\dot{\theta}S_\theta S_\phi + \dot{\psi}\dot{\phi}C_\theta C_\phi \\
\dot{r} &= -\ddot{\theta}S_\phi - \dot{\theta}\dot{\phi}C_\phi + \ddot{\psi}C_\theta C_\phi - \dot{\psi}\dot{\theta}S_\theta C_\phi - \dot{\psi}\dot{\phi}C_\theta S_\phi
\end{aligned} \quad \text{...(A.6)}$$

Order of magnitude analysis of the solution to C_{Tx}

The aerodynamic model considered in the analysis is composed of stability derivatives obtained for level trimmed flight at 20 m/s. Consider a typical co-ordinated maneuver where the angle of attack lies within ±10° and the airspeed does not significantly deviate from 20 m/s.

https://doi.org/10.1017/aer.2018.99 Published online by Cambridge University Press

Outside these bounds, the validity of the aerodynamic model itself is questionable. The order of magnitude of various quantities are estimated below:

$$\begin{aligned} QS &\sim 10^2 \\ C_L &\sim 10^{-1} \quad \Rightarrow \quad L \sim F_z \sim 10^1 \\ (a_0, a_1 a_2) &\sim 10^{-2} \quad \Rightarrow \quad D \sim F_x \sim 10^0 \end{aligned} \qquad \text{...(A.7)}$$

From (15), we get

$$f_1 \sim 10^{-1}, \quad f_2 \sim 10^{-2} \qquad \text{...(A.8)}$$

This gives us the order of magnitude of the terms in the solution to (17):

$$C_{Tx} = \Lambda \pm \sqrt{\Lambda^2 - \Xi} \qquad \text{...(A.9)}$$

$$\begin{aligned} \Lambda &= \left(\frac{a_1 S_\alpha + 2a_2 f_1 S_\alpha + C_\alpha}{2a_2 S_\alpha^2} \right) \sim 10^4 \\ \Xi &= \left(\frac{a_0 + a_1 f_1 + a_2 f_1^2 + f_2}{a_2 S_\alpha^2} \right) \sim 10^2 \end{aligned} \qquad \text{(A.10)}$$

Therefore, the solution with the positive square-root term is discarded as it yields a physically infeasible value for C_{Tx}.

Table A1
Stability and control derivatives of the aircraft

Parameter	Value	Parameter	Value
$C_{D0} + \tilde{C}_{D0}$	0.0173	C_{lp}	−0.673
C_{D1}	−0.0337	C_{lr}	0.113
C_{D2}	0.0517	$C_{l\delta_a}$	−0.691
$C_{Y\beta}$	−0.428	$C_{l\delta_r}$	−0.021
C_{Yp}	0.021	C_{m0}	0.069
C_{Yr}	0.279	$C_{m\alpha}$	−0.392
$C_{Y\delta_a}$	0.131	C_{mq}	−36.383
$C_{Y\delta_r}$	−0.391	$C_{m\delta_f}$	1.075
C_{L0}	0.312	$C_{m\delta_e}$	−2.195
$C_{L\alpha}$	5.926	$C_{n\beta}$	0.122
C_{Lq}	8.240	C_{np}	−0.036
$C_{L\delta_f}$	3.508	C_{nr}	−0.081
$C_{L\delta_e}$	0.384	$C_{n\delta_a}$	−0.045
$C_{l\beta}$	–0.029	$C_{n\delta_r}$	0.116

REFERENCES

1. THOMSON, D. and BRADLEY, R. Inverse simulation as a tool for flight dynamics research principles and applications, *Progress in Aerospace Sciences*, 2006, **42**, (3), pp 174–210.
2. ROUCHON, P., MARTIN, P. and MURRAY, R.M. *Flat systems, equivalence and trajectory generation, Tech. Rep. CDS 2003-008*, California Institute of Technology, Pasadena, California, USA, 2003.

https://doi.org/10.1017/aer.2018.99 Published online by Cambridge University Press

3. FLIESS, M., LÉVINE, J., MARTIN, P. and ROUCHON, P. Flatness and defect of non-linear systems: introductory theory and examples, *International J of control*, 1995, **61**, (6), pp 1327–1361.
4. NIEUWSTADT, M.J.V. and MURRAY, R.M. Real-time trajectory generation for differentially flat systems, *Int J of Robust and Nonlinear Control*, 1998, **8**, (11), pp 995–1020.
5. PETIT, N., MILAM, M.B. and MURRAY, R.M. Inversion based constrained trajectory optimisation, *IFAC Proceedings Volumes*, 2001, **34**, (6), pp 1211–1216.
6. YAKIMENKO, O.A. Direct method for rapid prototyping of near-optimal aircraft trajectories, *J of Guidance, Control, and Dynamics*, 2000, **23**, (5), pp 865–875.
7. DEITTERT, M., RICHARDS, A., TOOMER, C.A. and PIPE, A. Engineless unmanned aerial vehicle propulsion by dynamic soaring, *J of Guidance, Control, and Dynamics*, 2009, **32**, (5), pp 1446–1457.
8. AKHTAR, N., WHIDBORNE, J.F. and COOKE, A.K. Real-time optimal techniques for unmanned air vehicles fuel saving, *Proceedings of the Institution of Mechanical Engineers, Part G: J of Aerospace Engineering*, 2011, **226**, (10), pp 1315–1328.
9. BOSLOUGH, M. Autonomous dynamic soaring platform for distributed mobile sensor arrays, *Sandia National Laboratories, Sandia National Laboratories, Tech. Rep. SAND2002-1896*, 2002.
10. LAWRANCE, N.R.J. and SUKKARIEH, S. A guidance and control strategy for dynamic soaring with a gliding uav, In *IEEE International Conference on Robotics and Automation, 2009. ICRA'09.*, 2009, pp 3632-3637.
11. SUKUMAR, P.P. and SELIG, M.S. Dynamic soaring of sailplanes over open fields, *J of Aircraft*, 2013, **50**, (5), pp 1420–1430.
12. FLANZER, T.C., BUNGE, R.A. and KROO, I.M. Efficient six degree of freedom aircraft trajectory optimisation with application to dynamic soaring, In *12th AIAA Aviation Technology, Integration, and Operations (ATIO) Conference and 14th AIAA/ISSM*, 2012, p 5622.
13. LIU, D.N., HOU, Z.X. and GAO, X.Z. Flight modeling and simulation for dynamic soaring with small unmanned air vehicles, *Proceedings of the Institution of Mechanical Engineers, Part G: Journal of Aerospace Engineering*, 2017, **231**, (4), pp 589–605.
14. MARTIN, P. *Contribution à l'étude des systèmes différentiellement plats*, PhD Thesis, École Nationale Supérieure des Mines de Paris, 1992.
15. STEVENS, B.L., LEWIS, F.L. and JOHNSON, E.N. *Aircraft Control and Simulation: Dynamics, Controls Design, and Autonomous Systems,* John Wiley & Sons, New Jersey, US, 2015.
16. CAZAURANG, F., BERGEON, B. and LAVIGNE, L. Modeling of a longitudinal disturbed aircraft model by flatness approach, In *Proceedings of AIAA Conference, Guidance, Navigation and Control*, 2003, pp 5478-5482.
17. HINES, G.H. *Nonlinear Three-Dimensional Trajectory Following: Simulation and Application*, PhD Thesis, California Institute of Technology, 2008.
18. COOKE, J.M., ZYDA, M.J., PRATT, D.R. and MCGHEE, R.B. Npsnet: flight simulation dynamic modeling using quaternions, *Presence: Teleoperators & Virtual Environments*, 1992, **1**, (4), pp 404–420.
19. BERNDT, J.S. Jsbsim: An open source flight dynamics model, in C++. In AIAA Modeling and Simulation Technologies Conference and Exhibit, 2004, p 4923.
20. SEQUEIRA, C.J., WILLIS, D.J. and PERAIRE, J. Comparing aerodynamic models for numerical simulation of dynamics and control of aircraft, In *44th AIAA Aerospace Sciences Meeting and Exhibit, AIAA* 2006, p 1254.
21. BOWER, G.C. *Boundary Layer Dynamic Soaring for Autonomous Aircraft: Design and Validation*, PhD Thesis, Stanford University Stanford, 2011.
22. DRELA, M. and YOUNGREN, H. Athena vortex lattice 3.36 user primer, 2017.
23. LIU, D.N., HOU, Z.X., GUO, Z., YANG, X.X. and GAO, X.Z. Optimal patterns of dynamic soaring with a small unmanned aerial vehicle, *Proceedings of the Institution of Mechanical Engineers, Part G: J of Aerospace Engineering*, 2017, **231**, (9), pp 1593–1608.
24. SACHS, G. and BUSSOTTI, P. *Application of optimal control theory to dynamic soaring of seabirds*, Springer, Massachusetts, US, 2005.
25. RIGATOS, G.G. *Nonlinear Control and Filtering Using Differential Flatness Approaches: Applications to Electromechanical Systems*, Springer, Switzerland, 2015.
26. FAHROO, F. and ROSS, I.M. Direct trajectory optimisation by a Chebyshev pseudospectral method, *J of Guidance, Control, and Dynamics*, 2002, **25**, (1), pp 160–166.

https://doi.org/10.1017/aer.2018.99 Published online by Cambridge University Press